

# Local strains, calorimetry, and magnetoresistance in adaptive martensite transition in multiple nanostrips of $\text{Ni}_{39+x}\text{Mn}_{50}\text{Sn}_{11-x}$ ( $x \leq 2$ ) alloys

A A Prasanna and Shanker Ram

Materials Science Centre, Indian Institute of Technology, Kharagpur 721 302, India

E-mail: [sram@matsc.iitkgp.ernet.in](mailto:sram@matsc.iitkgp.ernet.in)

Received 6 August 2012

Accepted for publication 6 November 2012

Published 13 February 2013

Online at [stacks.iop.org/STAM/14/015004](http://stacks.iop.org/STAM/14/015004)

## Abstract


$\text{Ni}_{39+x}\text{Mn}_{50}\text{Sn}_{11-x}$  ( $x = 0.5, 1.0, 1.5$  and  $2$ ) alloys comprise multiple martensite nanostrips of nanocrystallites when cast in small discs, for example,  $\sim 15$  mm diameter and 8 mm width. A single martensite phase with a  $L1_0$  tetragonal crystal structure at room temperature can be formed at a critical Sn content of 9.0 at.% ( $x = 2$ ), whereas an austenite cubic  $L2_1$  phase turns up at smaller  $x \leq 1.5$ . The decrease in the Sn content from  $x = 2$  to 0.5 also results in a gradual increase in the crystallite size from 11 to 17 nm. Scanning electron microscopy images reveal arrays of regularly displaced multiple martensite strips ( $x \geq 1.5$ ) with an average thickness of 20 nm. As forced oscillators, these strips carry over the local strains, magnetic dipoles, and thermions simultaneously in a martensite–austenite (or reverse) phase transition. A net residual enthalpy change  $\Delta H_{M \leftrightarrow A} = -0.12 \text{ J g}^{-1}$  arises in the process that lacks reversibility between the cooling and heating cycles. A large magnetoresistance of  $(-)\text{26\%}$  at 10 T is observed together with a large entropy change of  $11.8 \text{ mJ g}^{-1} \text{ K}^{-1}$ , nearly twice the value ever reported in such alloys, in the isothermal magnetization at 311 K. The  $\Delta H_{M \leftrightarrow A}$  irreversibility accounts for a thermal hysteresis in the electrical resistivity. Strain induced in the martensite strips leads them to have a higher electrical resistivity than that of the higher-temperature austenite phase. A model considering time-dependent enthalpy relaxation explains the irreversibility features.

Keywords: Heusler alloys, martensite transition, magnetocaloric effect, magnetoresistance

## 1. Introduction

The martensite transition in ferromagnetic Ni–Mn–Sn Heusler alloys adapts unique properties of the shape-memory effect, inverse magnetocaloric effect, and magnetoresistance (MR) [1–11]. Functional properties crop up when structural transition coincides with a magnetic transition in the first-order diffusionless martensite transition, which is

mediated through a thermoelastic strain arising in a shear-like atomic displacement. A fine compositional detuning from a stoichiometric  $\text{Ni}_2\text{MnSn}$  Heusler alloy results in a phase transition from a cubic (austenite, A) to a tetragonal/orthorhombic (martensite, M) structure near room temperature. Although it is yet unclear why non-stoichiometry is required for the martensite transition, a theoretical prediction [6] explains the features by excess  $\text{Mn}(3d^54s^2)$  over  $\text{Ni}(3d^84s^2)$  as follows. The cubic phase is destabilized with a tetragonal distortion when the local electronic structure changes by hybridization between 3d orbitals of the excess Mn atoms at the Sn and Ni sites. Despite

 Content from this work may be used under the terms of the Creative Commons Attribution-NonCommercial-ShareAlike 3.0 licence. Any further distribution of this work must maintain attribution to the author(s) and the title of the work, journal citation and DOI.

extensive studies of magnetism and the magnetocaloric effect in  $\text{Ni}_{50}\text{Mn}_{50-x}\text{Sn}_x$  ( $5 \leq x \leq 25$ ) [1–3, 8–11], there are very few reports on electrical resistivity in alloys with  $13 \leq x \leq 16$  [4, 5, 7]. A ferromagnetic reordering occurs in a narrow  $x = 13$ – $15$  range, resulting in a ferromagnetic to paramagnetic transition in the martensite phase at the Curie point,  $T_C^M$ , before a reverse ferromagnetic reordering takes place at the martensite to austenite transition temperature,  $T_A$ .

A large difference between magnetizations in the martensite and austenite phases in such Ni–Mn–Sn alloys results in a large inverse magnetocaloric effect and magnetic shape memory. The transition carries over a large thermoelastic strain and a small irreversibility in spin reordering. A concurrent magnetic transition near room temperature is required for applications. In  $\text{Ni}_{50}\text{Mn}_{50-x}\text{Sn}_x$ , the martensite transition falls either well below or above room temperature [4, 5, 7, 12, 13]. Also a Ni-deficient  $\text{Ni}_{50-x}\text{Mn}_{39+x}\text{Sn}_{11}$  ( $5 \leq x \leq 7$ ) alloy exhibits a large gap (30 K at  $x = 5$ , or 80 K at  $x = 7$ ) between the two transitions and the transitions occur at temperatures  $T_M \sim 190$  K at  $x = 7$  or  $\sim 260$  K at  $x = 5$  [14], which are well below room temperature. Another  $\text{Ni}_{43-x}\text{Mn}_{47+x}\text{Sn}_{10}$  ( $x \leq 5$ ) series, which were studied as Ni-deficient alloys, has a  $T_M$  value well below room temperature [15]. In this system, the gap between  $T_M$  and the Curie point  $T_C^A$  (austenite) increased from 20 K at  $x = 0$  to as much as 170 K at  $x = 5$ .

In the  $\text{Ni}_{50}\text{Mn}_{50-x}\text{Sn}_x$  ( $5 \leq x \leq 25$ ) phase diagram [3], the valence–electron concentration  $e/a$  (8.0–8.2 per atom) controls the structural and magnetic transitions that approach each other very closely at  $e/a \sim 8.0$ . In this paper, we study multiple nanostrips (of crystallites) in  $\text{Ni}_{39+x}\text{Mn}_{50}\text{Sn}_{11-x}$  alloys ( $x = 0.5, 1.0, 1.5$  and 2) with  $e/a$  varying sharply from 7.87 to 7.96, which is smaller than that (8.0) proposed in the phase diagram. As  $x$  approaches 2.0 ( $e/a \rightarrow 7.96$ ), the two transitions concur with a large entropy change, nearly twice the value ever reported in such alloys, in alliance to a large MR at  $\sim 311$  K. A local strain that the nanostrips restore and carry over imparts a magnetocaloric peak to the  $A \rightarrow M$  transition. A thermal hysteresis in electrical resistivity and an enthalpy loss in the reverse transition arise due to a lack of reversibility in spin reordering.

## 2. Experimental details

The nanostrips of  $\text{Ni}_{39+x}\text{Mn}_{50}\text{Sn}_{11-x}$  ( $0.5 \leq x \leq 2$ ) were grown by cooling a melt in the shape of a disc (15 mm diameter and 8 mm width) in a mould of copper in a tungsten inert-gas arc-melting furnace. A master alloy made by melting and casting a stoichiometric mixture of pure metals in small discs was flipped and remelted three, four times ensuring a homogeneous mixing. The final compositions were measured using inductively coupled plasma optical emission spectroscopy (JY-ULTIMA spectrophotometer, France) and energy dispersive x-ray analysis performed with a Jeol JSM-5800 scanning electron microscope. Rectangular bars were freshly sliced from middle parts of the alloy discs by electrodischarge machining for x-ray diffraction (XRD) measurements. The measurements were carried out with

a high-resolution diffractometer (X'Pert PRO PANalytical) operated at 40 kV and 40 mA, using filtered 0.15410 nm  $\text{Cu}K_\alpha$  radiation. Nanostrips were observed in a field emission scanning electron microscope (FESEM, Zeiss SUPRA-40) at an accelerated voltage of 10 kV. Vickers microhardness was measured using a microhardness tester (UHL VMHT, Germany) with a load of 200 gf, at three different locations (including the disc center) with a 4 mm gap on the cross-section of the alloy disc sliced through the diameter. The heat outputs in the  $M \leftrightarrow A$  phase transitions were studied by heating and cooling a specimen at  $10 \text{ K min}^{-1}$  in a differential scanning calorimeter (DSC Q100, TA Instruments). Electrical resistivity ( $\rho$ ) was studied over the 10–300 K range using a standard four-probe method (Lakeshore Hall effect measurement instrument) by passing 100 mA of dc current through a sample of  $10 \times 1 \times 1 \text{ mm}^3$  size. Magnetic field ( $B$ ) dependent isothermal magnetization and  $\rho$  were studied using a superconducting quantum interface device and a physical properties measurement system (Quantum design), respectively, with  $B$  varied up to 10 T.

## 3. Results and discussion

### 3.1. Local strains and microstructure in nanostrips

The XRD patterns shown in figures 1(a)–(d) reveal distinct changes in the number and/or relative intensities of the peaks when varying the Sn content as  $x = 0.5, 1.0, 1.5$ , or 2.0 in  $\text{Ni}_{39+x}\text{Mn}_{50}\text{Sn}_{11-x}$  alloys marked as alloys 1, 2, 3, or 4, respectively. A simple pattern of only six peaks arises in a pure tetragonal  $L1_0$  martensite phase in alloy-4, with lattice parameters  $a = 0.7808 \text{ nm}$ ,  $c = 0.6954 \text{ nm}$  and density  $d = 7.797 \text{ g cm}^{-3}$  ( $z = 8$  formula units). As many as fifteen XRD peaks occur in a  $L2_1$  cubic crystal structure with the superlattice peaks (all  $h, k, l$  are odd) in alloy-1, with  $a = 0.6039 \text{ nm}$  and  $d = 7.615 \text{ g cm}^{-3}$  ( $z = 4$ ). The superlattice peaks no longer persist when the Ni content is raised, i.e. decreasing the Sn content to  $\sim 10$  at.% ( $x = 1$ ), in a strain-free fcc- $L2_1$  lattice having an enhanced  $d = 7.696 \text{ g cm}^{-3}$  ( $a = 0.6034 \text{ nm}$ ). With Ni increasing further, the  $L1_0$  phase ( $a = 0.7884 \text{ nm}$  and  $c = 0.6841 \text{ nm}$ ) co-precipitates with a simple fcc  $L2_1$  phase ( $a = 0.5980 \text{ nm}$ ) at an intermediate Sn content of 9.5 at.%. A compressive strain that develops in an intergranular structure in both phases enhances the densities by 0.2–2.0% over the values in the single-phase alloys 1 and 4.

When reinforced by the martensite phase ( $\sim 29$  vol% as per the XRD data of figure 1(c)) an austenite phase compresses greatly in the lattice volume ( $V$ ) by 3 versus 0.28% for the martensite phase (filler) because of a counterpart effect. This is a result of a surface-reinforced densification when one phase bounds the other phase with a rigid interface. A larger atomic radius of Sn (0.1405 nm) over Ni (0.1240 nm) results in a volume increase upon the  $\text{Sn} \rightarrow \text{Ni}$  substitution in a base  $\text{Ni}_{41}\text{Mn}_{50}\text{Sn}_9$  alloy. Phenomenologically, the substitution takes place primarily in the austenite phase. In table 1, consistently, a large  $\tau$  value of 3.5% (estimated from inhomogeneous broadening in the

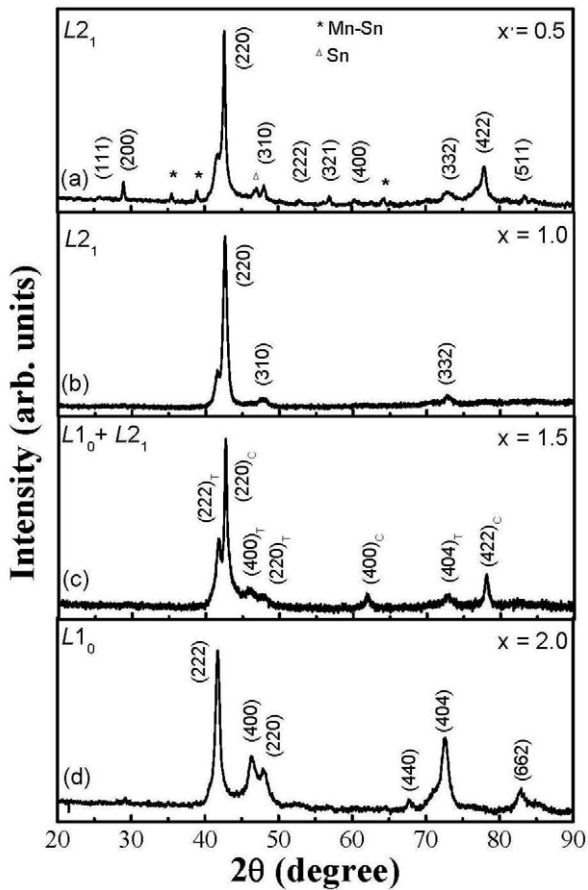


**Figure 1.** XRD patterns (a)–(d) reflecting the transformation from (a) a cubic austenite  $L2_1$  to (d) a tetragonal martensite  $L1_0$  phase in  $\text{Ni}_{39+x}\text{Mn}_{50}\text{Sn}_{11-x}$  ( $x \leq 2.0$ ) crystallites.

XRD peaks [16]) arises in a hybrid composite of two phases with 9.5 at.% of Sn. It reduces the average crystallite size to  $D = 12$  nm in comparison to a single austenite phase with  $D = 17$  nm. Other structural parameters computed from XRD patterns in the different alloys are included in table 1.

The FESEM images in figures 2(a) and (b) show martensite nanostrips in  $\text{Ni}_{39+x}\text{Mn}_{50}\text{Sn}_{11-x}$  alloys ( $x \geq 1.5$ ) grown in parallel arrays. As shown in figure 2(a), the strips in an XRD-pure martensite phase are separated by a distance of  $S_{ss}^M \sim 0.4 \mu\text{m}$  and have a thickness of  $S_{st}^M \sim 0.70 \pm 0.05 \mu\text{m}$ . These strips are grown preferentially in the (222) planes as judged from the most intense (222) peak in figure 1(d), viz. perpendicular to the [111] direction. While cooling a molten alloy, a liquid alloy phase splits up and solidifies in the multiple strips as a result of a directional cooling in thin rods ( $\sim 15$  mm or smaller diameter). The specific lattice volume ( $V_{sl}$ ) decreases by 2.3% (table 1) during the  $A \rightarrow M$  transition that imposes a compressive shear stress leading to a local splitting of the martensite phase into discrete and deep strips. To balance the compositional gradient, a primarily nondiffusional  $A \rightarrow M$  transition sets up with a restoring force. As a result, the strips persist when the alloy is cooled from a dynamic equilibrium at a critical temperature  $T_0$  with a decreased Gibbs free energy  $\Delta G_{A \rightarrow M} = \Delta V_{sl} \Delta G_V$ , where  $\Delta G_V$  is the Gibbs free-energy (per unit volume) of the transformation. A self-accommodating microstructural

behavior of the resulting alloy can arise in slipping and/or twinning in the local structure so as the strain-energy relieves in a pure martensite structure (figure 1(d)). A small (0.5 at.%) Sn inclusion above a pure martensite phase thus creates a compressive stress with  $S_{st}^M$  compressed by  $\sim 29\%$ , or  $V_{sl}$  by 2.3%, in a martensite–austenite alloy composite ( $x = 1.5$ ). The contraction of the strips with  $S_{ss}^M$  reduced by 50% increases the density of strips. An elastic energy that the strips store during the  $A \rightarrow M$  transition creates a compressive stress with *in situ* generated shear forces, which sets up a dynamic interfacial motion between the strips. A frictional force opposite to the interfacial motion, which boosts up when the  $S_{ss}^M$  drops adiabatically, compels the strips to split up into finer strips ( $S_{st}^M \sim 0.1 \mu\text{m}$ ) displaced between the parent strips ( $S_{st}^M$ ), as observed in figure 2(b). At  $x < 1.5$ , the strips disappear as soon as the martensite phase converts to the austenite phase near room temperature (figures 2(c) and (d)).

The FESEM images shown in figures 3(a)–(d) reveal that the  $\text{Ni}_{39+x}\text{Mn}_{50}\text{Sn}_{11-x}$  ( $2.0 \geq x \geq 1.5$ ) anisotropic bars consist of smaller substrips (4–16 in different regions). The region A of figure 3(a) ( $x = 2.0$ ) enlarged in figure 3(c) displays the substrips (thin laminates) displaced in regular arrays, which represent a nanotwinned structure (a mirror-like stacking fault of the close-packed atomic layers) in the martensite  $L1_0$  phase. In figures 3(b) and (d), less distinct laminates appear when two phases breed a net residual strain in an intergranular structure ( $x = 1.5$ ). The nanotwins arise to overcome the lattice mismatch with entities in the intimate contacts. Figure 3(e) shows the model substrips of a rectangular bar as they are observed in the FESEM images in figure 3(c), with an average thickness of 20 nm. A geometrical theory of martensite by Wechsler *et al* [17] predicts a periodic twinning of a tetragonal lattice, expressed through the fraction of the twin lamellar widths  $w_1$  and  $w_2$  as  $w_1/w_2 = (a_m - a_a)/(a_a - c_m)$ , where  $a_m$ ,  $c_m$ , and  $a_a$  are the lattice parameters with the subscripts m and a denoting martensite and austenite. The values  $a_m = 0.7884$ ,  $c_m = 0.6954$  nm, and  $a_a = 0.6039$  nm calculated from XRD patterns imply  $w_1/w_2 \approx 2$ , illustrating that periodically arranged nanotwin lamellae, with  $w_1:w_2 = 2:1$ , can interbridge martensite strips as modeled in figure 3(f). The bright ( $\sim 20$  nm) and dark (10 nm) strips have thicknesses in the same ratio,  $w_1:w_2 = 2:1$ .

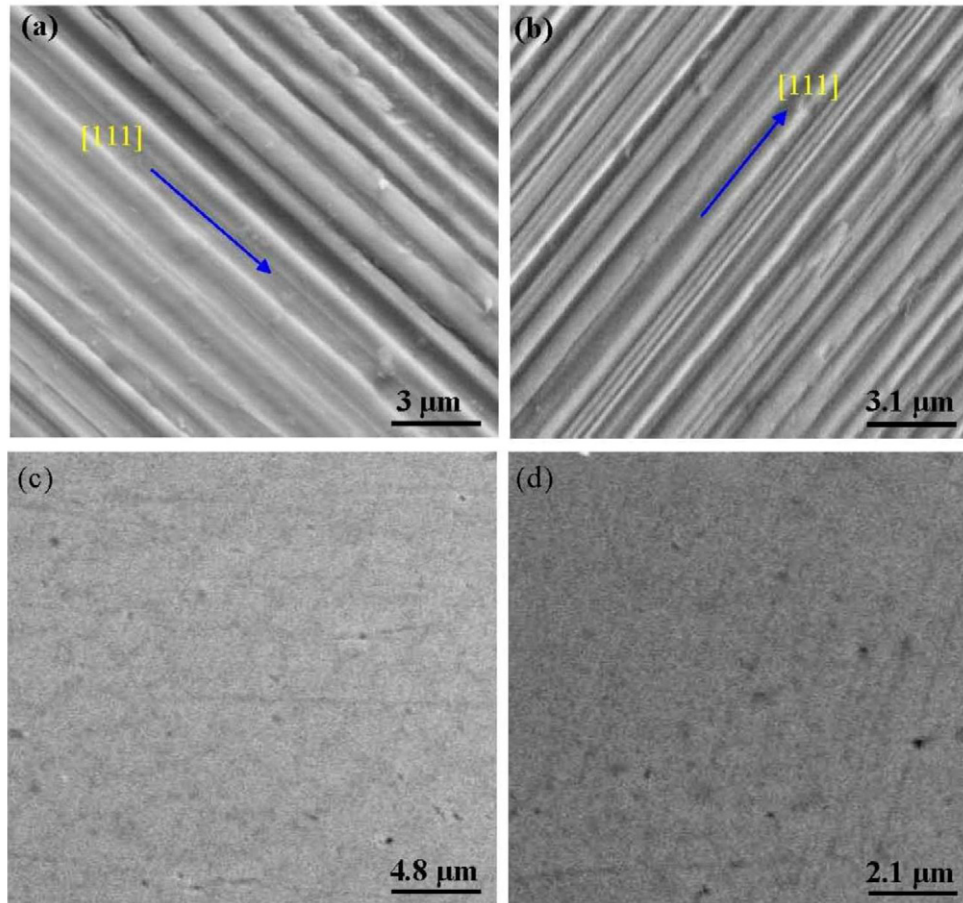
### 3.2. Vickers microhardness

To explore whether the composition and microstructure control the mechanical hardness in  $\text{Ni}_{39+x}\text{Mn}_{50}\text{Sn}_{11-x}$  ( $x \leq 2.0$ ), we studied Vickers microhardness ( $H_V$ ) at three different points on a vertical cross-section sliced from a disc, viz. close to (i) the upper (U) and (ii) lower (L) surfaces by 1.0 mm from the lateral faces and (iii) the midpoint (C). As shown in figure 4, the  $H_V$  value has an inverse relation with  $\tau$  value, an atypical effect of the local strain on the alloy hardening. In Hooke's law, the hardness is directly proportional to the local strain, i.e. the strain increases linearly against the stress within the elastic limit. A deviation arises here because the martensite strips that are pinned down at the nanotwins govern

**Table 1.** Structural parameters in martensite and austenite  $\text{Ni}_{39+x}\text{Mn}_{50}\text{Sn}_{11-x}$  ( $x \leq 2.0$ ) phases.

| $x$ | $e/a$ | Phase            | Lattice parameters (nm) |        | $D$<br>(nm) | $\tau$<br>(%) | $V$<br>( $\text{nm}^3$ ) | $d$<br>( $\text{g cm}^{-3}$ ) | $V_{\text{sl}}$<br>( $\text{cm}^3 \text{g}^{-1}$ ) |
|-----|-------|------------------|-------------------------|--------|-------------|---------------|--------------------------|-------------------------------|--|
|     |       |                  | $a$                     | $c$    |             |               |                          |                               |  |
| 0.5 | 7.87  | $L2_1(\text{A})$ | 0.6039                  | –      | 17          | 2.5           | 0.2202                   | 7.615                         | 0.1315   |
| 1.0 | 7.90  | $L2_1(\text{A})$ | 0.6034                  | –      | 13          | 0.9           | 0.2197                   | 7.696                         | 0.1300   |
| 1.5 | 7.93  | $L2_1(\text{A})$ | 0.5980                  | –      | 12          | 3.5           | 0.2138                   | 7.766                         | 0.1290   |
|     |       | $L1_0(\text{M})$ | 0.7808                  | 0.6841 | –           | –             | 0.4240                   | 7.812                         | 0.1280   |
| 2.0 | 7.96  | $L1_0(\text{M})$ | 0.7884                  | 0.6954 | 11          | 1.7           | 0.4252                   | 7.797                         | 0.1285   |

The values are accurate to the last reported digits, except  $V_{\text{sl}}$  within  $\pm 0.05\%$  error.


**Figure 2.** FESEM images showing that martensite  $\text{Ni}_{39+x}\text{Mn}_{50}\text{Sn}_{11-x}$  strips (a)  $x = 2.0$  and (b)  $x = 1.5$  disappear on conversion to an austenite phase at (c)  $x = 1.0$  and (d)  $x = 0.5$ .

the average value. As shown in table 2, the average  $H_V$  value 2.584 GPa ( $x = 2.0$ ) is smaller compared to the values for  $x \leq 1.0$  because of a significantly weak interfacial motion and weak pinning between effectively thick strips. The  $H_V$  value falls down by 13% when the pinning weakens further in the same kinds of strips in a mixed M–A phase ( $x = 1.5$ ). A similar elastic softening is shown in ferroelastic domains that are pinned down weakly in the cubic  $\rightarrow$  tetragonal phase transition in  $\text{SrTiO}_3$ ,  $\text{KMnF}_3$ , or  $\text{KMn}_{0.997}\text{Ca}_{0.003}\text{F}_3$  at temperatures below 200 K [18,19]. In the  $\text{Ni}_{39+x}\text{Mn}_{50}\text{Sn}_{11-x}$  ( $x \leq 2.0$ ) series, a single austenite phase ( $x = 1.0$ ) that grows at the expense of the interface with a residual martensite phase acquires a larger hardness  $H_V = 3.321$  GPa, but a smaller residual strain  $\tau = 0.9\%$ . Further, when a superlattice

structure builds up with a local strain, the  $H_V$  drops marginally in the alloy-1 ( $x = 0.5$ ).

The  $H_V$  values compared in table 2 for different regions of four  $\text{Ni}_{39+x}\text{Mn}_{50}\text{Sn}_{11-x}$  ( $x = 0.5, 1.0, 1.5$  and 2) alloys are the averaged values measured on three discs prepared under the same conditions. They were reproducible within a standard deviation of  $\pm 0.2\%$ , illustrating the veracity of the hardness variation across the disc. The outer region, which had cooled faster in a bulk structure, is a softer austenite phase. During cutting from a disc, a compressive stress in the lower surface would breed surface hardening only. The hardness propagates with local strain that relieves when the martensite phase splits up and self-accommodates as illustrated with the FESEM image of figure 2(a).

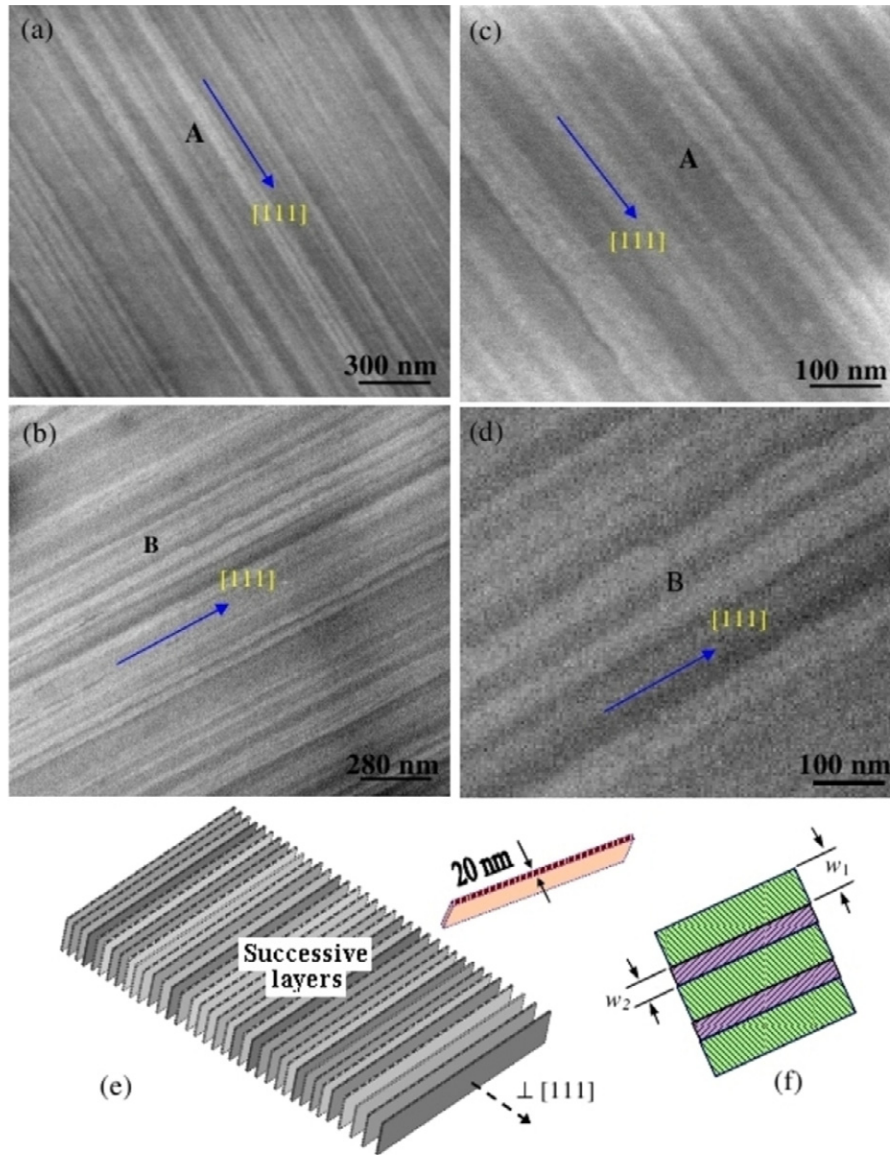


**Figure 3.** FESEM images showing bundles of multiple martensite strips (4–16 thin laminates in different regions) in  $\text{Ni}_{39+x}\text{Mn}_{50}\text{Sn}_{11-x}$  at (a)  $x = 2.0$  and (b)  $x = 1.5$ , with enlarged parts (c) A and (d) B. (e) A model pattern of laminates (f) of nanotwinned atomic layers.

### 3.3. Calorimetric signals in magnetostructural transitions

Now let us analyze how the martensite strips and local strains affect the caloric signals jointly in the magnetic and structural transitions. The heat output was measured during heating followed by cooling the  $\text{Ni}_{39+x}\text{Mn}_{50}\text{Sn}_{11-x}$  alloy ( $x \leq 2$ ) in the temperature range 200–400 K. The results so obtained are compared in figure 5 for three alloys ( $x = 1.0, 1.5$ , and  $2.0$ ). Upon heating, an exothermic peak ( $x \geq 1.5$ ) appears at temperature  $A_p$  in the  $M \rightarrow A$  transition, with  $A_p > T_A$ , where  $T_A = (A_s + A_f)/2$  is a midpoint of the austenite start  $A_s$  and austenite finish  $A_f$  temperatures. A modified transition peak occurs at  $M_p > T_M$  on cooling, where  $T_M$  is a midpoint of the martensite start  $M_s$  and finish  $M_f$  temperatures. In other words, both endothermic and exothermic peaks are asymmetric, and show a hysteresis  $\Delta T = A_p - M_p$ . At  $x \sim 2.0$ , the  $T_M = 310.5$  K and  $T_A = 322.5$  K are raised considerably above room temperature with

a strong caloric signal of an enthalpy change  $\Delta H_{M \leftarrow A} = 3.325 \text{ J g}^{-1}$ , or entropy  $\Delta S_{M \leftarrow A} = 10.655 \text{ mJ kg}^{-1} \text{ K}^{-1}$ , and full-width at half maximum  $\beta_{M \leftarrow A} = 29.7$  K. The local strains ( $\tau = 1.7\%$ ) relieved in regular martensite strips have a higher  $\Delta H_{M \leftarrow A}$  value compared to samples with  $x = 1$  or  $1.5$  (table 3). Reheating gives a smaller  $\Delta H_{M \rightarrow A} = 3.205 \text{ J g}^{-1}$ , or  $\Delta S_{M \rightarrow A} = 9.800 \text{ mJ g}^{-1} \text{ K}^{-1}$ , in the process that lacks reversibility in the enthalpy, which is relieved slowly when the paramagnetic martensite state reverts back to the ferromagnetic austenite state. A thermal variation that sets up in the electrical conduction is modified in a spin disorder  $\rightarrow$  reorder transition. In comparison to Ni-rich alloys  $\text{Ni}_{49}\text{Mn}_{38}\text{Sn}_{13}$  ( $8.35 \text{ J g}^{-1}$ ) and  $\text{Ni}_{50}\text{Mn}_{35}\text{Sn}_{15}$  ( $5.1 \text{ J g}^{-1}$ ) [3, 20], these  $\Delta H_{M \leftarrow A}$  values are smaller, but correspond to a larger  $\beta_{M \leftarrow A} \sim 29.7$  K and a higher transition temperature ( $T_M = 310.5$  K), 2.2 times the temperature in  $\text{Ni}_{45}\text{Co}_5\text{Mn}_{40}\text{Sn}_{10}$  of an intermediate Ni content (bulk  $L1_0$  phase;  $T_M = 130$  K) [21].

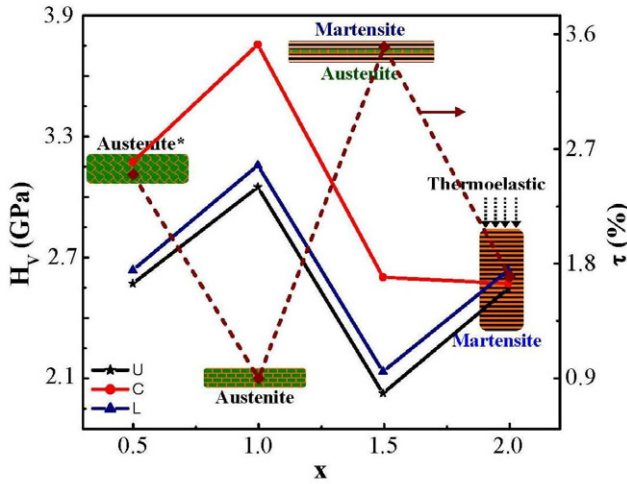


**Figure 4.** Vickers microhardness ( $H_V$ ) showing martensite ( $x = 2.0$ ) and austenite ( $x = 1.0$ ) phase softening at the expense of strains  $\tau$  in  $\text{Ni}_{39+x}\text{Mn}_{50}\text{Sn}_{11-x}$  crystallites. The data were measured on upper (U), central (C) and lower (L) cross-sections from an alloy disc. \*Contains superlattices.

**Table 2.** Vickers microhardness ( $H_V$ ) and gradient ( $\partial H_V/\partial y$ ) in  $\text{Ni}_{39+x}\text{Mn}_{50}\text{Sn}_{11-x}$  ( $x \leq 2.0$ ) alloys.

| x   | $H_V$ (GPa) |       |       | $\partial H_V/\partial y$ (GPa mm $^{-1}$ ) |                  |
|-----|-------------|-------|-------|---|------------------|
|     | U           | C     | L     | U $\rightarrow$ C                           | C $\leftarrow$ L |
| 0.5 | 2.570       | 3.175 | 2.635 | 0.200                                       | 0.180            |
| 1.0 | 3.050       | 3.755 | 3.155 | 0.235                                       | 0.200            |
| 1.5 | 2.025       | 2.605 | 2.135 | 0.190                                       | 0.155            |
| 2.0 | 2.545       | 2.570 | 2.635 | 0.010                                       | 0.020            |

The data are measured on upper (U), central (C) and lower (L) cross-sections of three discs. The values are correct with  $\pm 0.2\%$  error.

As shown by the hatched areas in the DSC peaks in figure 6(a), the martensite strips ( $x = 2.0$ ) in cooling and heating exhibit not only a large irreversibility  $\Delta H_{M \leftarrow A} - \Delta H_{M \rightarrow A} = 0.120 \text{ J g}^{-1}$  ( $\Delta G_{M \rightarrow A} = \Delta H_{M \rightarrow A} \Delta T / 2T_0 \cong 70.490 \text{ mJ g}^{-1}$ , with  $T_0 = \frac{1}{2}(M_s + A_f)$ ), but also a thermal hysteresis ( $\Delta T = 15.1 \text{ K}$ ). Possible contributions to these effects arise from (i) well-displaced twinned martensite strips (figure 3(f)) that bear a strong magnetic spin-pinning barrier, (ii) residual stress on a granular structure, (iii) spin relaxation, (iv) magnetoelastic coupling between spins and lattice ordering, (v) thermal conductivity induced in dynamic spins and phonons, and (vi) different heat capacities in the two states ( $\Delta C_P^{M \leftrightarrow A}$ ). Further, the strips divide the sample into domains by spins pin-down at the boundaries. A local spin-lattice reconfiguration that sets up in a transition thus adds a large frictional energy (or shear and compressive stresses) according to a large  $\Delta H_{M \leftarrow A} = 3.325 \text{ J g}^{-1}$  found in this alloy. Low electrical resistivity and stress in the austenite state ease a spin-lattice heat transfer in an exchange-coupled relaxation that drives *in situ* spin disorder (paramagnetic martensite)  $\leftarrow$  order (ferromagnetic austenite) transition by absorbing a large  $\Delta H_{M \leftarrow A}$  over a large span  $\beta_{M \leftarrow A}$  with  $\Delta C_P^{M \leftarrow A} \sim 0.090 \text{ mJ g}^{-1} \text{ K}^{-1}$ .

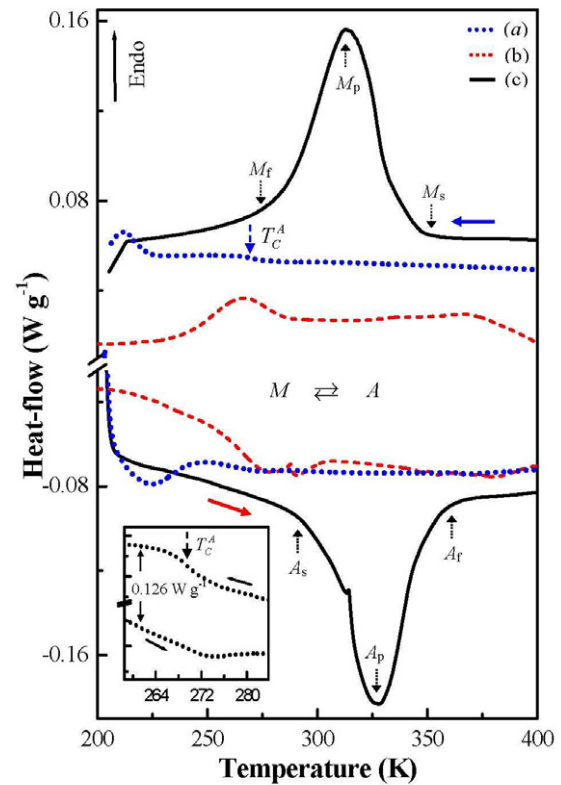


**Figure 5.** DSC thermograms for the  $M \leftrightarrow A$  transition in cooling and heating of  $\text{Ni}_{39+x}\text{Mn}_{50}\text{Sn}_{11-x}$  at  $10 \text{ K min}^{-1}$  in argon; (a)  $x = 1.0$ , (b)  $x = 1.5$ , and (c)  $x = 2.0$ . Martensite strips ( $x = 2.0$ ) exhibit prominent peaks while only a weak signal is observed near  $T_C^A$  in the austenite ( $x = 1.0$ , see the inset).

A model  $C_P$ -diagram in figure 6(b) explains a positive  $\Delta C_P^{M \leftarrow A} = C_P(M_f) - C_P(M_s)$  value assuming a spin-lattice relaxation relieves heat before a heat uptake begins in the  $M \leftarrow A$  transition from a point  $A_e$  (cooling). The heat dissipates faster in the conductive A-state. After the transition terminates at  $M_f$ , the  $C_P$  rises up further due to the spins disorder in a paramagnetic phase  $M_e$ . In reheating from point  $M_e$ , a value  $\Delta C_P^{M \rightarrow A} = C_P(A_s) - C_P(A_f) \cong 0.068 \text{ mJ g}^{-1} \text{ K}^{-1}$  evolves, i.e. expectedly lower than  $0.090 \text{ mJ g}^{-1} \text{ K}^{-1}$  observed in the transition in cooling, following part of the heat relieved in a spin-lattice relaxation. As indicated in figure 6(b), a  $C_P$  value of  $0.270 \text{ mJ g}^{-1} \text{ K}^{-1}$  estimated at  $M_f$  ( $> T_C^M$ ) from the DSC thermograms (figure 6(a)) is raised to  $0.311 \text{ mJ g}^{-1} \text{ K}^{-1}$  upon heating to  $A_s$ . For a fixed ratio  $\kappa_e/\gamma$  ( $\kappa_e$  = electronic thermal conductivity and  $\gamma$  = electrical conductivity) in the Wiedemann-Franz law in a metal, a diminished  $\kappa_e$  value in the martensite strips accounts for the energy loss in a spin-lattice heat transfer, describing a lower  $\Delta C_P^{M \rightarrow A} < \Delta C_P^{M \leftarrow A}$ . A lower magnetization ( $\sigma$ ) thus increases in the A-phase by 58% in a low magnetic field  $B = 5 \text{ mT}$ , or 12% in  $B = 5 \text{ T}$ .

Qualitatively,  $\kappa_e$  enhanced in a mixed M/A phase  $\text{Ni}_{39+x}\text{Mn}_{50}\text{Sn}_{11-x}$  ( $x = 1.5$ ) yields smaller  $\Delta C_P^{M \leftarrow A} - \Delta C_P^{M \rightarrow A}$ ,  $\Delta H_{M \leftarrow A} - \Delta H_{M \rightarrow A} = 0.095 \text{ J g}^{-1}$ ,  $\Delta G_{M \rightarrow A} = 6.325 \text{ mJ g}^{-1}$ , and  $\Delta T = 11.1 \text{ K}$  (figure 6(c)). The residual martensite that transforms into austenite near 383 K (or the reverse transition near 367 K in the cooling cycle) leads to

**Table 3.** M ↔ A caloric transition parameters in Ni<sub>39+x</sub>Mn<sub>50</sub>Sn<sub>11-x</sub> (x ≤ 2.0) alloys.

| x   | RT phase                          | A <sub>p</sub> (K) | M <sub>p</sub> (K) | ΔT (K) | ΔH (J g <sup>-1</sup> ) |        | ΔS (mJ g <sup>-1</sup> K <sup>-1</sup> ) |        | ΔG (mJ g <sup>-1</sup> ) |         |
|-----|-----------------------------------|--------------------|--------------------|--------|-------------------------|--------|--|--------|--------------------------|---------|
|     |                                   |                    |                    |        | M ← A                   | M → A  | M ← A                                    | M → A  | M ← A                    | M → A   |
| 1.0 | L21                               | 225.0              | 212.0              | 13.0   | 0.130                   | -0.155 | 0.615                                    | -0.695 | 3.640                    | -4.310  |
| 1.5 | L2 <sub>1</sub> + L1 <sub>0</sub> | 276.2              | 265.1              | 11.1   | 0.435                   | -0.340 | 1.645                                    | -1.225 | 8.155                    | -6.325  |
| 2.0 | L2 <sub>1</sub>                   | 327.1              | 312.0              | 15.1   | 3.325                   | -3.205 | 10.655                                   | -9.800 | 73.110                   | -70.490 |

RT: room temperature. The A<sub>p</sub>, M<sub>p</sub>, and ΔT are accurate within ±0.5 K error, while other entities within ±0.1% of the reported values.

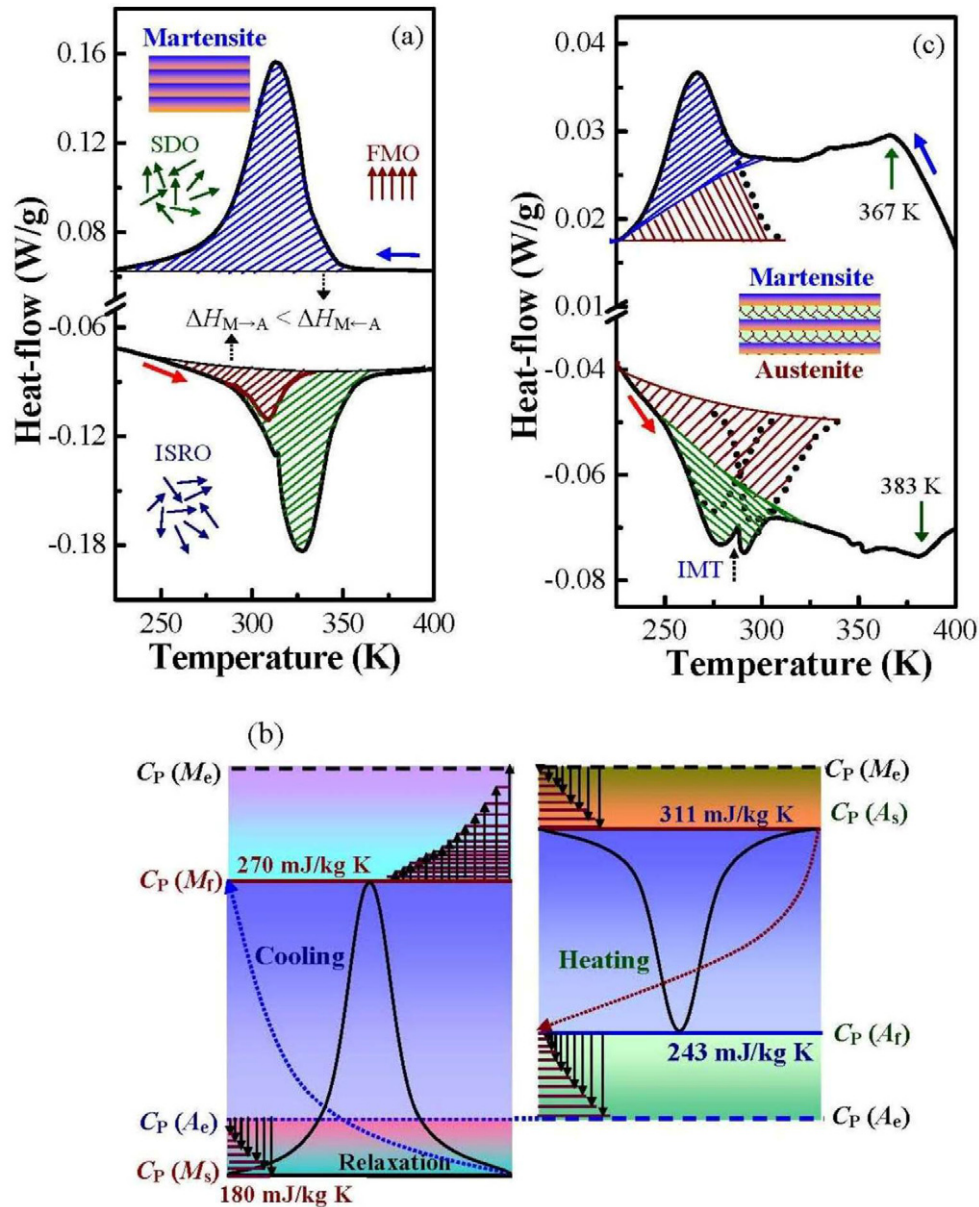


**Figure 6.** DSC signals with irreversible ΔH in M ↔ A transition for x = 2 (a) and 1.5 (c). (b) A model Cp-diagram in Ni<sub>39+x</sub>Mn<sub>50</sub>Sn<sub>11-x</sub> (x = 2.0). An IMT peak appears with a weak signal in a premartensite transition (marked by the vertical arrows in (c) in a mixed phase (x = 1.5). FMO: ferromagnetic ordering, SDO: spin disordering; ISRO: irreversible spin-reordering.

a superimposition of the DSC signal over a background due to the local structural changes. A similar phase transition between the micromodulated phase and a bcc austenite is known in Ni<sub>2</sub>MnGa near 230 K, but with a smaller ΔT ≈ 7 K [22]. For x ≥ 1.5, T<sub>C</sub><sup>A</sup> and T<sub>M</sub> (or T<sub>A</sub>) coincide

in a single caloric signal, while a distinct T<sub>C</sub><sup>A</sup> appears near 270 K (figure 5(a)) at x = 1.0. An intermartensite transition (IMT) emerges in a distinct signal at lower temperature to the martensite transition peak, at 288 K for 9.5 at.% Sn (x = 1.5), or 315 K for 9.0 at.% Sn (x = 2.0). Any internal stress that

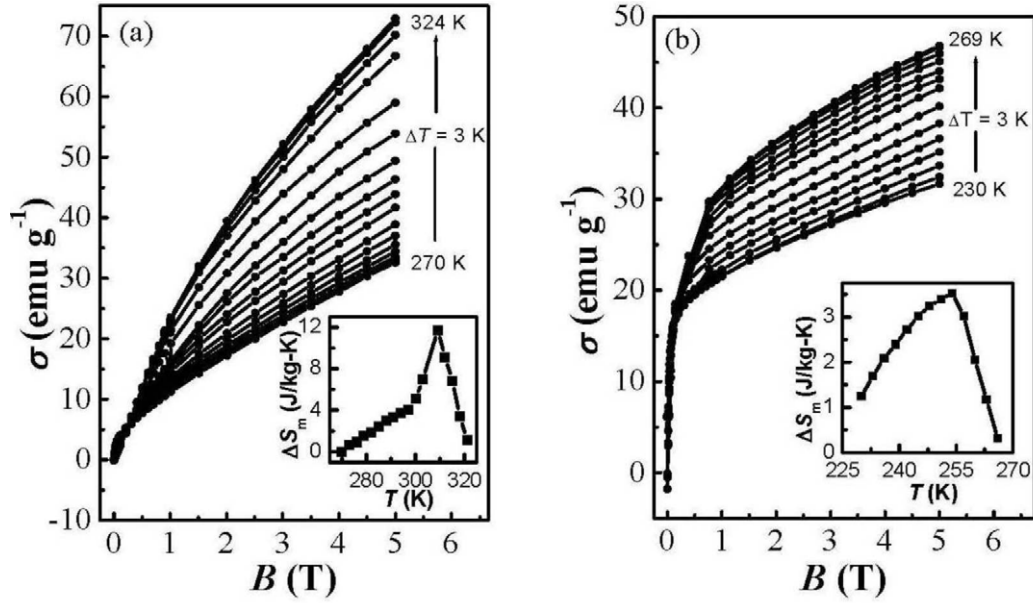


**Figure 7.** Magnetization isotherms with a  $\sigma$  jump in the  $M \rightarrow A$  transition in  $\text{Ni}_{39+x}\text{Mn}_{50}\text{Sn}_{11-x}$ ; (a)  $x = 2.0$  and (b)  $x = 1.5$ , with a larger  $\Delta S_m$  in martensite strips ( $x = 2.0$ ) in the insets.

builds up during the local atomic redistribution is relieved in this process [23]. A characteristically faster  $\Delta H$  change accounts for a stronger IMT signal in the  $M \leftarrow A$  transition (cooling).

The martensite strips  $\text{Ni}_{39+x}\text{Mn}_{50}\text{Sn}_{11-x}$ ,  $1.5 \leq x \leq 2.0$ , assist both the  $\Delta C_p^{M \leftrightarrow A}$  irreversibility and magnetocaloric effect. As shown in figures 7(a) and (b), upon heating from 309 to 312 K the  $\sigma$  value in the  $x = 2.0$  alloy that exhibits a large irreversibility is enhanced by as much as  $7.1 \text{ emu g}^{-1}$  in  $B = 5 \text{ T}$ . This increase corresponds to a large magnetic entropy change  $\Delta S_m = 11.8 \text{ mJ g}^{-1} \text{ K}^{-1}$ , or refrigerant capacity  $\text{RC} = 133.1 \text{ mJ g}^{-1}$ , near  $T_A \sim 312 \text{ K}$  in an inverse magnetocaloric effect in the standard relation

$$\Delta S_m = \sum_i \frac{\sigma_{i+1}(T_{i+1}, B) - \sigma_i(T_i, B)}{T_{i+1} - T_i} \Delta B. \quad (1)$$

A larger  $T_A$  of 322.5 K is observed in DSC revealing that magnetic field shifted the transition to lower temperatures. The RC was calculated from the area under the  $\Delta S_m$  versus  $T$  curve (inset in figure 7(a)) in a field of 5 T. Only a residual  $\Delta S_m \sim 3.5 \text{ mJ g}^{-1} \text{ K}^{-1}$  ( $\text{RC} \sim 105.3 \text{ mJ g}^{-1}$ ) lasts due to the reduction in the  $\Delta C_p^{M \leftrightarrow A}$  irreversibility in a mixed M/A phase ( $x = 1.5$ ) near  $T_A \sim 254 \text{ K}$ , viz. the irreversibility helps the magnetocaloric effect. A minor austenite phase also suppresses  $\Delta S_m$  to  $\sim 1.0 \text{ mJ g}^{-1} \text{ K}^{-1}$  ( $\Delta B = 9 \text{ T}$ ) in the  $\text{Ni}_{50}\text{Mn}_{34}\text{Sn}_{16}$  alloy ( $T_M = 190 \text{ K}$ ) [13]. Pure martensite strips are thus required to enhance  $\Delta S_m$ .

### 3.4. Forced oscillations and damping in multiple martensite strips

Let us consider that a compressive stress induced by thermal agitation in the  $M \leftarrow A$  transition compels substrips in a group to oscillate about their average positions. As small oscillators they carry over the local strains, magnetic dipoles,

and thermions along effective force  $F$  exerted on the strips. A strip thus obeys the following equation of motion in a single degree of freedom:

$$m \frac{d^2 y}{dt^2} + h \frac{dy}{dt} + \alpha y = F_0 \sin \omega t, \quad (2)$$

with  $F = F_0 \sin \omega t$ , where  $F_0$  is the oscillation amplitude,  $\omega$  is angular frequency,  $m$  is the mass of a strip,  $h$  is the effective damping coefficient,  $\alpha$  is the dynamic restoring coefficient in a strip, and  $y$  is displacement from the mean position;  $h$  arises from the internal friction between the strips  $\text{Ni}_{39+x}\text{Mn}_{50}\text{Sn}_{11-x}$ . Qualitatively, a larger value  $h_{M \leftarrow A}$  arises in the  $M \leftarrow A$  transition because the oscillators transfer the strain, spin, and thermion from a low-strain point ( $M_s$ ) to a higher value ( $M_f$ ). A model diagram in figures 8(a)–(d) according to the observed  $\Delta H_{M \leftarrow A}$  (DSC) indicates that the initial  $h_{M \leftarrow A}$  decays faster with time  $t$  than  $h_{M \rightarrow A}$  on the heating. Lesser interfacial friction in the strips decreases the damping ( $h_{M \rightarrow A} < h_{M \leftarrow A}$ ) so that the separation of strips no longer ceases rapidly. Here,  $m$  is constant and  $\alpha$  is a weak function of time.

A phase difference  $\phi$  between the force and resultant motion  $y = R \sin(\omega t - \phi)$  in an oscillator of amplitude  $R$  gives on substituting in equation (2),

$$\frac{y\alpha}{F_0} = \frac{\sin(\omega t - \phi)}{\sqrt{\left(1 - \frac{\omega^2}{\omega_n^2}\right)^2 + (2\xi\omega/\omega_n)^2}} = R_d \sin(\omega t - \phi), \quad (3)$$

with  $\xi = h/h_c$ , where  $h_c$  is the critical  $h$  value at which transmissibility  $\Gamma$  of spins and thermions approaches zero, and  $\omega_n$  is the natural frequency of the strips. One can express

$$\phi = \tan^{-1} \left( \frac{2\xi\omega/\omega_n}{1 - \omega^2/\omega_n^2} \right). \quad (4)$$

Here,  $R_d$  is a dimensionless response factor,  $\sim 1$  at very low  $\omega$  values. It traces a peak near  $\omega_n$  and approaches zero as



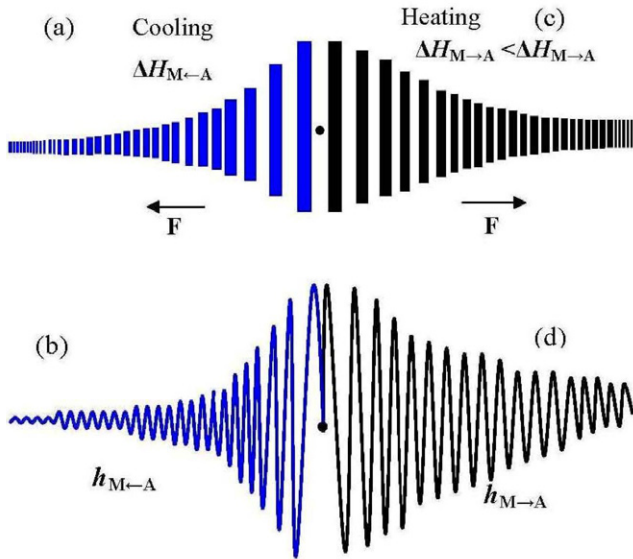


**Figure 8.** Model damping of collective oscillations of multiple martensite strips under a compressive force during (a, b) cooling and (c, d) heating via an  $M \leftrightarrow A$  transition in  $\text{Ni}_{39+x}\text{Mn}_{50}\text{Sn}_{11-x}$  ( $x \leq 2.0$ ). Damping coefficient  $h_{M \rightarrow A}$  modified during heating induces irreversibility in the process parameters.

$\omega \rightarrow \infty$ . The force that transmits through the strips in carrying over the strain, spin, and thermion can be expressed in a differential equation

$$F_T = h \frac{dy}{dt} + \alpha y. \quad (5)$$

The forces  $h dy/dt$  and  $\alpha y$  are phase-shifted by  $90^\circ$ , and thus the  $F_T$  magnitude is

$$|F_T| = \sqrt{h^2 \frac{d^2 y}{dt^2} + \alpha^2 y^2}. \quad (6)$$

The ratio  $\frac{F_T}{F_0} = \Gamma \sin(\omega t - \psi)$  implies

$$\Gamma = \sqrt{\frac{1 + (2\xi \omega / \omega_n)^2}{(1 - \omega^2 / \omega_n^2)^2 + (2\xi \omega / \omega_n)^2}}, \quad (7)$$

$$\psi = \tan^{-1} \frac{2\xi(\omega / \omega_n)^3}{1 - (\omega / \omega_n)^2 + 4(\xi \omega / \omega_n)^2}. \quad (8)$$

Equation (7) results in a weak peak in figure 9(A) with  $\Gamma \leq 5$  at resonance  $\omega / \omega_n = 1$  for  $\xi \geq 0.1$  in an  $M \leftarrow A$  transition. This peak is intensified for a smaller  $\xi = 0.01$ , which is possible if strains and thermions flow collectively and rapidly with spins from a disordered configuration (lower  $\kappa_c$ ) before the  $M_f$  sets in. A moderate  $\xi$  value on smaller  $h$  in a reverse transition gives a medium  $\Gamma$  peak. A maximum  $\psi$  determined in a wide transition over  $1 \leq \omega / \omega_n \leq 10$  transmits a maximum energy (figure 9(B)).

As shown in figure 10(A), a net force in the oscillators can describe an ellipse  $F = \alpha R \sin \omega t + h \omega R \cos \omega t$ . It dissipates the following amount of heat energy per unit time:

$$\frac{\partial H}{\partial t} = \int_{\mu}^{\mu+2\pi/\omega} F \frac{dy}{dt} dt = \pi \omega \xi^3 R^2. \quad (9)$$

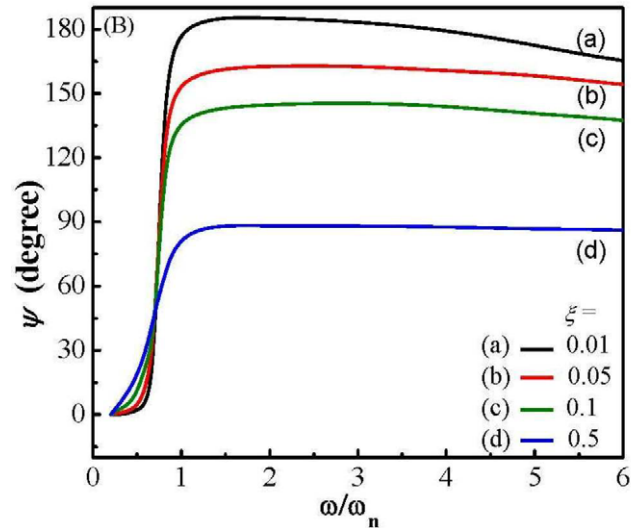
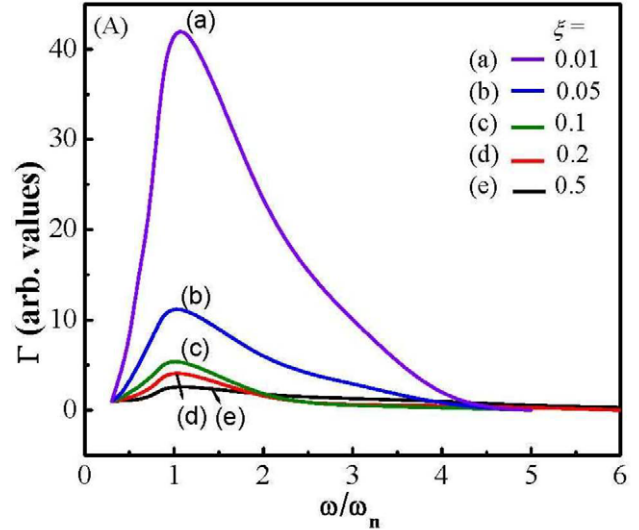


**Figure 9.** Variations of (A) transmissibility and (B) phase angle against  $\omega / \omega_n$  when the damping parameter  $\xi$  is varied from 0.01 to 0.5.

Analogous to equation (3),  $\omega$  and  $\xi$  in a collective oscillation of the strips of period  $\mu$  describe

$$R = \frac{F_0 / \alpha}{\sqrt{\left(1 - \frac{\omega^2}{\omega_n^2}\right)^2 + (2\xi \omega / \omega_n)^2}}. \quad (10)$$

Integrating equation (9) between  $\mu$  and  $\mu + 2\pi \omega^{-1}$  yields

$$\frac{\partial H}{\partial t} = \frac{\chi \pi \omega \xi^3 F_0^2 / \alpha^2}{\left(1 - \frac{\omega^2}{\omega_n^2}\right)^2 + (2\xi \omega / \omega_n)^2} \quad (11)$$

or

$$\frac{\partial H}{\partial t} = \frac{z \omega \xi^3}{\left(1 - \frac{\omega^2}{\omega_n^2}\right)^2 + (2\xi \omega / \omega_n)^2}, \quad (12)$$

where  $z = \chi \pi h_c F_0^2 / \alpha^2$  is a constant and  $\chi$  is a correlation factor. As shown in figure 10(B), a normalized  $\partial H / \partial t$  with  $z = 1$  has a peak against  $\omega / \omega_n$  in an  $M \leftarrow A$  transition. As

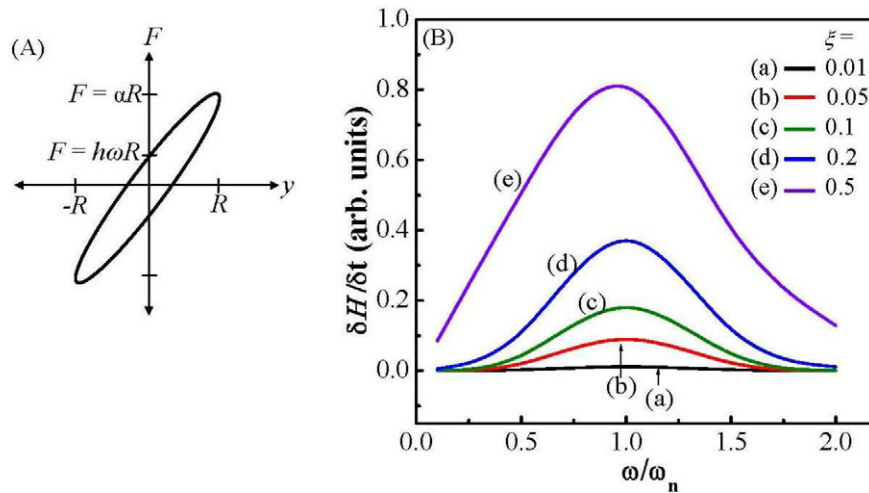


**Figure 10.** (A) Phase diagram of a damped oscillator and (B) the rate of the enthalpy change  $\partial H/\partial t$  versus normalized frequency  $\omega/\omega_n$  from equation (12).

$\omega/\omega_n \rightarrow 1$ , the  $\partial H/\partial t$  reaches a maximum at a nodal point, i.e., the  $T_M$  or  $T_A$  point. The peak intensity rises progressively with the parameter  $\xi$  used in figure 9. As a result, considering an average  $\xi$  value can corroborate a weaker heat flow as it is observed when cooling the sample.

### 3.5. Magnetoresistance and entropy in magnetostructural transition

To illustrate the effects of the local structural and magnetic changes on the  $M \leftrightarrow A$  transitions in terms of electrical transport in  $\text{Ni}_{39+x}\text{Mn}_{50}\text{Sn}_{11-x}$  ( $x \leq 2.0$ ), we studied  $\rho$  and MR in different conditions as follows. In figure 11,  $\rho$  displays a thermal hysteresis in cooling and heating, with a more resistive structure on the heating damping heat flow with moderate  $\xi$  value. For  $x \sim 2.0$ , the  $\rho$  value rises sharply in the  $M \leftarrow A$  transition at  $T_M \sim 309$  K (table 4) due to enhanced local strains and spin disordering, which promotes electron scattering. A large change  $\Delta\rho_{M \leftarrow A} = 275 \mu\Omega \text{ cm}$  along with  $\kappa_e = LT/\rho$  is changed by  $\Delta\kappa_e^{M \leftarrow A} = \kappa_e(M_s) - \kappa_e(M_f) \cong 2.49 - 1.06 = 1.43 \text{ W m}^{-1} \text{ K}^{-1}$  using the Lorentz number  $L = 2.45 \times 10^{-8} \text{ W } \Omega^{-1} \text{ K}^{-2}$  in the Wiedemann–Franz law. On heating, the transition results in a release of thermoelastic energy in a large  $\rho$ – $T$  hysteresis  $(\rho T)_h = 17.5 \text{ m}\Omega \text{ cm K}$ , or  $\Delta T = T_A - T_M \sim 15$  K. This sizeable irreversibility is important for tailoring MR and other properties. At  $x \sim 1.5$ , impeded strips turn up in the  $M \leftarrow A$  transition with a large residual strain (3.5%) resulting in a lowered  $\Delta\rho_{M \leftarrow A} = 62 \mu\Omega \text{ cm}$ , or  $\Delta\kappa_e^{M \leftarrow A} = \kappa_e(M_s) - \kappa_e(M_f) \cong 1.24 - 0.82 = 0.42 \text{ W m}^{-1} \text{ K}^{-1}$ .  $(\rho T)_h$  is markedly lowered to  $1.85 \text{ m}\Omega \text{ cm K}$  ( $\Delta T \sim 9.5$  K) in a transient fashion in the reverse transition. Relatively smaller strains stored on low irreversibility in the transition cycles result in average  $(\rho T)_h = 5.5 \text{ m}\Omega \text{ cm K}$  at  $x = 1.0$ , or  $3.6 \text{ m}\Omega \text{ cm K}$  at  $x = 0.5$ . The slope of the  $\rho$ – $T$  curve changes at the  $T_C^A \sim 265$  K ( $x = 0.5$ ), or  $270$  K for  $x \sim 1$ .

Figure 12 shows the field dependence of  $\rho$  values at temperatures between 100 and 320 K in  $\text{Ni}_{39+x}\text{Mn}_{50}\text{Sn}_{11-x}$  of low ( $x \sim 2$ ) and high ( $x \sim 1.5$ ) strains. The data were

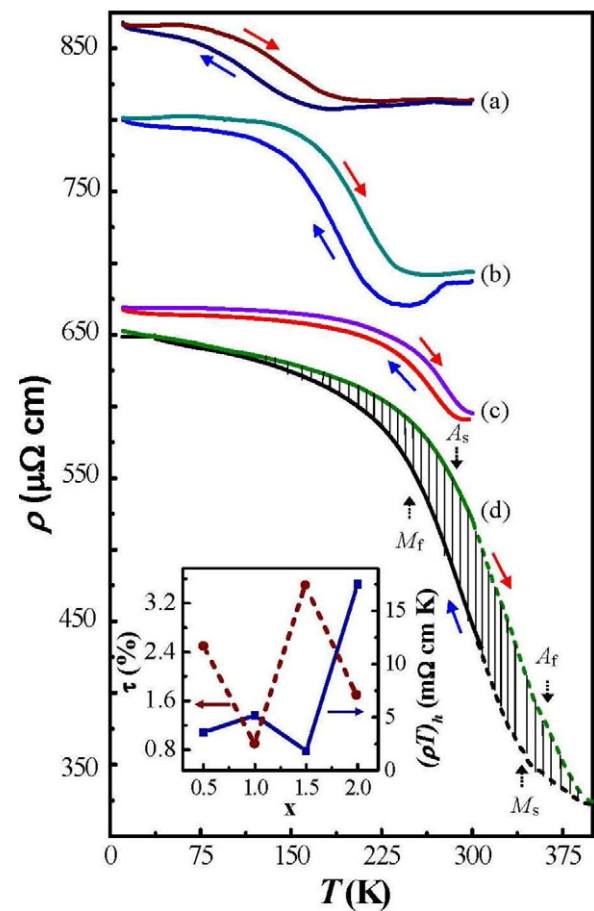


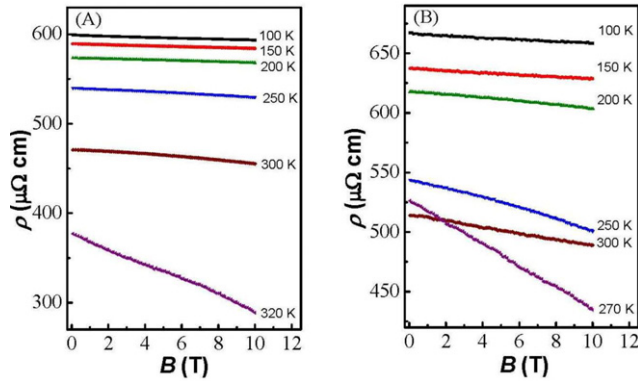
**Figure 11.** Thermal hysteresis in the  $M \leftrightarrow A$  transition in electrical resistivity  $\rho$  of  $\text{Ni}_{39+x}\text{Mn}_{50}\text{Sn}_{11-x}$ : (a)  $x = 0.5$ , (b)  $x = 1.0$ , (c)  $x = 1.5$ , and (d)  $x = 2.0$ . The martensite strips ( $x = 2.0$ ) exhibit a large hysteresis loss  $(\rho T)_h$  plotted in the inset. The given  $\rho$ -scale applies to the sample  $x = 2.0$ ; it is to be divided by 2.55, 2.28, or 0.97 for the  $x = 0.5, 1.0$  or  $1.5$  samples.

measured by warming a zero-field-cooled sample from 100 K. A large MR =  $-26\%$  arises near  $T_A \sim 320$  K (figure 12(A)) in  $B = 10$  T for a low strain of 1.7%. The MR decreases

**Table 4.** Martensite transition temperatures measured from DSC thermograms and  $\rho$ - $T$  hystereses in  $\text{Ni}_{39+x}\text{Mn}_{50}\text{Sn}_{11-x}$  ( $x \leq 2.0$ ) alloys.

| $x$ | Method      | $M_s$ (K) | $M_f$ (K) | $A_s$ (K) | $A_f$ (K) | $T_M$ (K) | $T_A$ (K) | $\Delta T$ (K) |
|-----|-------------|-----------|-----------|-----------|-----------|-----------|-----------|----------------|
| 0.5 | Resistivity | 163       | 79        | 102       | 172       | 121.0     | 137.0     | 15.0           |
| 1.0 | DSC         | 222       | —         | —         | 242       | —         | —         | 13.0           |
|     | Resistivity | 220       | 178       | 166       | 240       | 189.0     | 203.0     | 14.0           |
| 1.5 | DSC         | 288       | 235       | 237       | 300       | 261.5     | 268.5     | 11.1           |
|     | Resistivity | 287       | 233       | 238       | 301       | 260.0     | 269.5     | 9.5            |
| 2.0 | DSC         | 334       | 287       | 297       | 348       | 310.5     | 322.5     | 15.1           |
|     | Resistivity | 337       | 283       | 295       | 350       | 309.0     | 324.0     | 15.0           |

The temperatures are accurate within  $\pm 0.5$  K error in general.

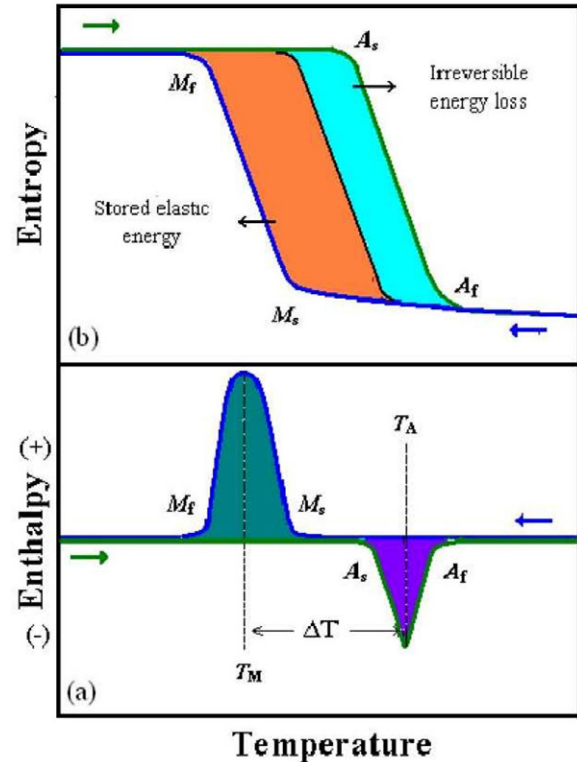

**Figure 12.** Magnetic field dependence of resistivity  $\rho$  in  $\text{Ni}_{39+x}\text{Mn}_{50}\text{Sn}_{11-x}$  with (A)  $x = 2.0$  and (B)  $x = 1.5$ . A lack of fully reversible spin reordering correlates with a large MR =  $(-)$ 26% in the  $M \rightarrow A$  transition ( $x = 2.0$ ) at 320 K and  $\Delta B = 10$  T.

to  $(-)$ 17% near  $T_A \sim 270$  K (figure 12(B)) for the higher strain of 3.5% in the other sample. While negative MR arises when  $B$  suppresses the spin-disorder scattering of electrons, a significantly large MR lasts if the spin reordering lacks reversibility in a strain-free system. Such large MR is useful for room-temperature applications. A still larger value  $(-)$ 50% is known in an alloy  $\text{Ni}_{50}\text{Mn}_{36}\text{Sn}_{14}$ , but at a low temperature of 150 K and in large  $B = 18$  T [4].

In the model enthalpy-temperature diagrams of figures 13(a) and (b), thermions propagate easily via martensite strips giving rise to a net change of enthalpy  $\Delta H$ , or entropy  $\Delta S$ , in a magnetostructural transition in  $\text{Ni}_{39+x}\text{Mn}_{50}\text{Sn}_{11-x}$  ( $x \leq 2$ ). This change contains three major parts of  $\Delta H_{\text{chem}}$  from a chemical change,  $\Delta H_{\text{elast}}$  from an elastic strain change, and irreversible change  $\Delta H_{\text{irr}}$  in the transition. The Gibbs free energy that leads to change the  $M \leftrightarrow A$  states yields  $\Delta H_{\text{chem}}$ , while  $\Delta H_{\text{elast}}$  arises in restoring the lattice volume. A nonzero  $\Delta H_{\text{irr}}$  value, requisite of a thermal hysteresis of the transition, describes the work done by the frictional forces opposing the interfacial motions in the strips in spin disordering or reordering. In this approximation, the final  $\Delta H$  value that an  $M \leftarrow A$  transition absorbs (cooling), or a reverse transition releases (heating), can be expressed as

$$\Delta H_{M \leftarrow A} = \Delta H_{\text{chem}}^{M \leftarrow A} + \Delta H_{\text{elast}}^{M \leftarrow A} + \Delta H_{\text{irr}}^{M \leftarrow A}, \quad (13)$$

$$\Delta H_{M \rightarrow A} = \Delta H_{\text{chem}}^{M \rightarrow A} + \Delta H_{\text{elast}}^{M \rightarrow A} + \Delta H_{\text{irr}}^{M \rightarrow A}. \quad (14)$$


**Figure 13.** Schematic of hystereses in (a) enthalpy and (b) entropy in the  $M \leftrightarrow A$  transitions in  $\text{Ni}_{39+x}\text{Mn}_{50}\text{Sn}_{11-x}$  ( $x \leq 2.0$ ) martensite strips.

If  $\Delta H_{\text{chem}}^{M \leftrightarrow A}$  dissipates rapidly, as observed in Cu-Al-X ( $X = \text{Zn}, \text{Ni}$ ) and Fe-Pt alloys [24], a reversibility  $\Delta H_{M \leftarrow A} > \Delta H_{M \rightarrow A}$  could develop in  $\text{Ni}_{39+x}\text{Mn}_{50}\text{Sn}_{11-x}$  ( $x \leq 2$ ) martensite strips due to a time lag in the  $\Delta H_{\text{irr}}^{M \leftrightarrow A}$  relaxation process over heating and cooling via the transition. It can be described with an empirical relation,  $\Delta H_{\text{irr}}^{M \rightarrow A} = \Delta H_{\text{irr}}^{M \leftarrow A} \exp \left\{ -(t_{\text{sp}}/t_{\text{st}})^N \right\}$ , where  $t_{\text{sp}}$  is the spin-relaxation time and  $t_{\text{st}}$  is the structural relaxation time with an exponent  $N$ . Setting  $N \sim 1$  and  $t_{\text{sp}} \ll t_{\text{st}}$  in an ergodic transition accounts for the reversibility. A fractional  $\Delta H_{M \rightarrow A} \sim 0.964 \Delta H_{M \leftarrow A}$  at  $x = 2.0$ , or  $0.775 \Delta H_{M \leftarrow A}$  at  $x = 1.5$ , observed by DSC in  $\text{Ni}_{39+x}\text{Mn}_{50}\text{Sn}_{11-x}$  is reproduced well with  $t_{\text{sp}}/t_{\text{st}} = 0.01$  and  $N = 0.72$ , viz. a nonergodic transition,  $t_{\text{sp}} < t_{\text{st}}$  and  $0 < N < 1$ , i.e. the time average of a physical quantity does not represent an estimate of the initial value. Arrested dynamics slow down relaxation of locally trapped carriers in such transitions [25]. Thus,

in the absence of full relaxation over the experimental timescale  $\Delta H_{\text{irr}}^{M \rightarrow A}$  and  $\Delta H_{\text{elast}}^{M \rightarrow A}$  exhibit a hysteresis in an entropy–temperature diagram, or a temperature lag  $\Delta T$  in an enthalpy–temperature diagram. A controlled spin relaxation which determines  $\Delta H_{\text{irr}}^{M \rightarrow A}$  is required in high-performance spintronics [26, 27].

#### 4. Conclusions

The  $\text{Ni}_{39+x}\text{Mn}_{50}\text{Sn}_{11-x}$  alloys where Ni is partially substituted by nonmagnetic Sn ( $x = 0.5, 1.0, 1.5,$  and  $2.0$ ) illustrate that an inverse magnetocaloric effect concurs with a large MR in the multiple martensite alloy nanostrips that transact the carriers in the  $M \leftrightarrow A$  transition. For an optimal Sn content of 9.0 at.% ( $x = 2.0$ ), the transition occurs well above room temperature, at  $T_M \sim 310.5$  K, from a cubic  $L2_1$  austenite phase ( $x \leq 1.0$ ) to a tetragonal  $L1_0$  martensite phase. A local strain, which builds up in the  $M \leftarrow A$  transition in cooling, propagates undisrupted through the anisotropic nanostrips that displace and transfer the energy as a forced oscillator. In a nanotwinning process, a martensite strip splits into a regular pattern of 4–16 substrips ( $\sim 20$  nm average thickness). The spins that are pinned down at the boundaries divide the substrips into the single magnetic domains. These spins also cause surface alloy hardening with effectively large shear stress, compressive stress, and frictional energy on account of a coupled spin–lattice system. A major part of the heat intake  $\Delta H_{M \leftarrow A} = 3.325 \text{ J g}^{-1}$ , such as  $3.205 \text{ J g}^{-1}$ , is relieved in the transition that reverts back (upon reheating) with reversibility of the heat carriers. A large  $\text{MR} = -26\%$  is observed and it carries over a large entropy change  $\Delta S_m \sim 11.8 \text{ mJ g}^{-1} \text{ K}^{-1}$ , nearly twice the value reported for such alloys [3, 20, 27]; this large MR is useful for room-temperature applications. The observed features degrade sharply on austenite phase precipitates ( $x \leq 1.5$ ). A model enthalpy–temperature diagram with a time-dependent spin–lattice–thermion relaxation in a nonergodic nature of the  $M \leftrightarrow A$  transition explains how a local strain is generated with the spins pin-down at the domain boundaries thereby enhancing the  $\Delta H_{M \leftrightarrow A}$  and  $\Delta S_m$  values.

#### Acknowledgments

AAP is thankful to AICTE, New Delhi, and Bahubali College of Engineering, Shravanabelagola, for a partial financial support of this work.

#### References

- [1] Sutou Y, Imano Y, Koeda N, Omori T, Kainuma R, Ishida K and Oikawa K 2004 *Appl. Phys. Lett.* **85** 4358
- [2] Krenke T, Duman E, Acet M, Wassermann E F, Moya X, Mañosa L and Planes A 2005 *Nature Mater.* **4** 450
- [3] Krenke T, Acet M, Wassermann E F, Moya X, Mañosa L and Planes A 2005 *Phys. Rev. B* **72** 014412
- [4] Koyama K, Okada H and Watanabe K 2006 *Appl. Phys. Lett.* **89** 182510
- [5] Khan M, Pathak A K, Paudel M R, Dubenko I, Stadler S and Ali A 2008 *J. Magn. Magn. Mater.* **320** L21
- [6] Ye M *et al* 2010 *Phys. Rev. Lett.* **104** 176401
- [7] Bose S K, Kudrnovsky J, Drchal V and Turek I 2011 *Phys. Rev. B* **84** 174422
- [8] Banerjee A, Chaddah P, Dash S, Kumar K, Lakhani A, Chen X and Ramanujan R V 2011 *Phys. Rev. B* **84** 214420
- [9] Umetsu R Y, Sheikh A, Ito W, Ouladdiaf B, Zeibek K R A, Kanomata T and Kainuma R 2011 *Appl. Phys. Lett.* **98** 042507
- [10] Han Z, Chen J, Qian B, Zhang P, Jiang X, Wang D and Du Y 2012 *Scr. Mater.* **66** 121
- [11] Basso V, Sasso C P, Skokov K P, Gutfleisch O and Khovaylo V V 2012 *Phys. Rev. B* **85** 014430
- [12] Chatterjee S, Giri S, Majumdar S and De S K 2008 *Phys. Rev. B* **77** 224440
- [13] Shamberger P J and Ohuchi F S 2009 *Phys. Rev. B* **79** 144407
- [14] Han Z D, Wang D H, Zhang C L, Xuan H C, Gu B X and Du Y W 2007 *Appl. Phys. Lett.* **90** 042507
- [15] Xuan H C, Zheng Y X, Ma S C, Cao Q Q, Wang D H and Du Y W 2010 *J. Appl. Phys.* **108** 103920
- [16] Qadri S B, Skelton E P, Hsu D, Dinsmore A D, Yang J, Gray H F and Ratna B R 1999 *Phys. Rev. B* **60** 9191
- [17] Wechsler M S, Lieberman D S and Read T A 1953 *Trans. Am. Inst. Min. Metall. Eng.* **197** 1503
- [18] Kityk A V, Schranz W, Sondergeld P, Havlik D, Salje E K H and Scott J F 2000 *Phys. Rev. B* **61** 946
- [19] Salje E K H and Zhang H 2009 *J. Phys.: Condens. Matter* **21** 035901
- [20] Babita I, Ram S, Gopalan R and Chandrasekaran V 2009 *Phil. Mag. Lett.* **89** 399
- [21] Srivastava V, Chen X and James R D 2010 *Appl. Phys. Lett.* **97** 014101
- [22] Planes A, Obrado E, Gonzalez-Comas A and Manosa L 1997 *Phys. Rev. Lett.* **79** 3926
- [23] Kaufmann S, Rößler U K, Heczko O, Wuttig M, Buschbeck J, Schultz L and Fähler S 2010 *Phys. Rev. Lett.* **104** 145702
- [24] Ortin J and Planes A 1988 *Acta Metall.* **36** 1873
- [25] Manno M, Bulone D, Martorana V and San Biagio P L 2004 *Physica A* **341** 40
- [26] Hai P N, Ohya S and Tanaka M 2010 *Nat. Nanotechnol.* **5** 593
- [27] Babita I, Patil S I and Ram S 2010 *J. Phys. D: Appl. Phys.* **43** 205002